

Structure and bonding in boron carbide: The invincibility of imperfections†

Musiri M. Balakrishnarajan,‡ Pattath D. Pancharatna and Roald Hoffmann*

Received (in Montpellier, France) 18th December 2006, Accepted 8th February 2007

First published as an Advance Article on the web 27th February 2007

DOI: 10.1039/b618493f

Boron carbide, usually described as B_4C , has the mysterious ability to accommodate a large variation in carbon composition (to as much as $B_{10}C$) without undergoing a basic structural change. We systematically explore how the bonding varies with carbon concentration in this structure and the origin of the fundamental electron deficiency of the phase. As the carbon concentration is reduced, we find that the *exo*-polyhedral $B_{Eq}-C$ bonds of the icosahedra in the structure become increasingly engaged in multiple bonding, and the repulsive steric interactions between the bulky B_{12} units surrounding the carbon atom are reduced. The short bond lengths observed within the three-atom $\equiv C-B-C \equiv$ chains are then due to substantial π -bonding, while the carbon deficiency weakens its σ -framework significantly. We conclude that the idealized framework of boron carbide has to expel some electrons in order to maximize its bonding; disorder in the structure is an inevitable consequence of this partial oxidation. The localization of electronic states arising from the disorder leads to the semiconducting nature of boron carbide throughout its composition range.

Introduction

The hardest substances are all covalent solids, mainly based on carbon, boron and nitrogen.¹ Boron carbide, long known,² with an extreme hardness of about 30 GPa,³ is inferior only to diamond and cubic-BN, but is less expensive and easier to prepare. At temperatures above 1200 °C its hardness is reported to even exceed that of diamond.⁴ Coupled with its high thermodynamic stability (m.p. ~ 2500 °C),⁵ low density (2.5 g cm^{-3}) and remarkable chemical inertness,⁵ boron carbide serves as an ideal choice for a variety of important applications.

Among boron-rich materials, boron carbide has become the most extensively used technically,⁶ it is being used in abrasive/shielding materials that sustain extreme conditions, such as light weight armor, and in nuclear reactors as a neutron absorber. It is also a promising material in high efficiency direct thermoelectric conversion⁷ and in special purpose doped semiconductors⁸ (though, so far, all doped boron carbides are only p-type semiconductors). The possibility of making superconducting materials⁹ and solid state neutron detectors¹⁰ based on the boron carbide family is also being explored.

Unfortunately, fundamental aspects of the bonding in boron carbide and the important structural changes caused by varying the carbon concentration are still not clearly understood. In fact, until now, even the detailed structure of boron carbide was not known unambiguously. In this inves-

tigation, we present an in-depth theoretical analysis of bonding in boron carbide, in an attempt to explain and resolve in a chemically meaningful manner many of the lingering questions and ambiguities about this fascinating material. Furthermore, we compare the bonding in a closely related stoichiometric structure, $LiB_{13}C_2$, where the covalent network is isomorphic to $B_{13}C_2$.¹¹

The structure and electron counting

In its idealized, most symmetric form, the structure of boron carbide is usually described in a rhombohedral unit cell (space group $R\bar{3}m$) that contains one icosahedral B_{12} unit and one linear $\equiv C-B-C \equiv$ chain, corresponding to the ideal composition $B_{13}C_2$. The B_{12} units are composed of crystallographically distinct boron atoms B_{Eq} (Equatorial) and B_P (Polar) in a D_{3d} environment. These B_{12} units are interconnected by carbon atoms through their B_{Eq} atoms, forming layers, while the B_{12} units of the adjacent layers are linked through interpolyhedral B_P-B_P bonds. Besides these two kinds of boron atoms in the icosahedron, there is a unique boron (B_C) that connects the two carbon atoms of the adjacent layers, forming the short linear $\equiv C-B-C \equiv$ chain. Fig. 1 depicts the hexagonal ($z = 2$) and rhombohedral ($z = 1$) forms of $B_{13}C_2$, along with a top view of the structure.

That structure is the ideal archetype, but boron carbide actually exists over a widely varying compositional range $B_{12+x}C_{3-x}$ ($0.06 < x < 1.7$).¹² Owing to the similarity of boron and carbon in electron density and nuclear cross-section (^{11}B and ^{12}C), both X-ray and neutron diffraction studies are not very successful in unambiguously assigning the exact site occupancies. It is generally agreed that the carbon and B_P sites (Fig. 1) exhibit mixed occupancies to varying degrees, depending on the carbon concentration.¹³ Besides, the three-atom

Department of Chemistry and Chemical Biology, Baker Laboratory, Cornell University, Ithaca, NY 14853, USA. E-mail: rh34@cornell.edu

† The HTML version of this article has been enhanced with additional colour images.

‡ Present address: Department of Chemistry, Pondicherry University, Pondicherry 605 014, India.

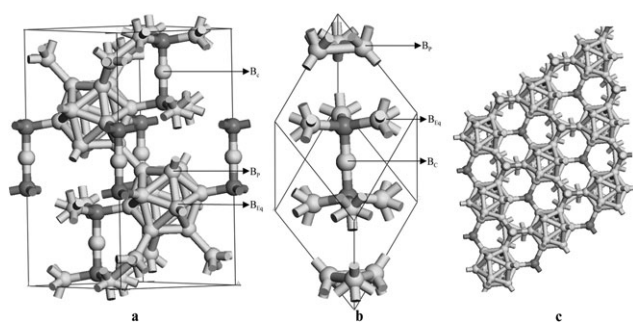


Fig. 1 The structure of $B_{13}C_2$ (a) hexagonal unit cell (b) rhombohedral unit cell (c) a top view of (a) showing B_{12} layers with perpendicular interstitial $\equiv C-B-C \equiv$ chains.

chains are reported to be partially occupied at low carbon concentrations.¹⁴ However, permanent interstitial occupations appear to be absent.

Let's turn to electron counting rules, so successful in polyhedral boron chemistry. All the bonds of carbon and the *exo*-polyhedral bonds of the B_{12} unit in boron carbide are generally considered to be single bonds. Since the B_{12} unit requires two electrons ($B_{12}H_{12}^{2-} - 12H\bullet$)¹⁵ and the divalent boron B_C needs to shed one of its electrons in its linear geometry, the $B_{13}C_2$ unit cell can be split up, for electron counting purposes, into (B_{12}^{2-}) ($\equiv C-B^+-C \equiv$). This electron counting scheme places a net -1 charge on $B_{13}C_2$; hence we refer to the neutral phase as electron-deficient. The replacement of any one of the boron atoms by carbon will lead to the electron-precise boron carbide $B_{12}C_3$ (or B_4C). Band structure calculations indeed show $B_{12}C_3$ to be a semiconductor with a definite gap¹⁶ and $B_{13}C_2$ to be metallic,¹⁷ as expected from the above electron counting scheme, but boron carbide is found experimentally to be a semiconductor throughout the range of its carbon concentration; its electronic properties are largely governed by hopping processes dominated by holes.¹⁸ However, measurements of magnetic susceptibility,¹⁹ ESR²⁰ and other related²¹ studies show very low spin densities.

Mysteries of boron carbide: structural issues and bonding controversies

Hiding behind the simple 15 atom unit cell of boron carbide is an array of puzzling facts and fundamental structural/bonding questions. One of the mysteries is the ability of the boron carbide structure to accommodate a large variation in carbon concentration (from B_4C to $B_{10}C$) without phase separation or interstitial occupancies. The relative thermodynamic stabilities of the different stoichiometries present a second challenge, already addressed in the literature by Bylander and co-workers.^{16,17}

Surprisingly, the ideal 'electron-precise' composition $B_{12}C_3$ has never been isolated experimentally. Electron deficient $B_{13}C_2$ is reported to melt congruently at 2450 and 2480 °C, while the most electron-rich composition ($\sim B_{12}C_3$) melts incongruently at 2350 and 2360 °C, indicating its comparative instability.²²

Besides these two anomalous observations, conflicting views exist concerning the nature of site occupancies. Initially, the

electron-rich composition ($\sim B_{12}C_3$) was reported by X-ray studies²³ to have a rhombohedral structure based on B_{12}^{2-} and $\equiv C-C^{2+}-C \equiv$ fundamental structural units. However, improved X-ray^{13,22,24} and neutron diffraction²⁵ studies, NMR analysis,²⁶ and theoretical calculations of the free energy,¹⁶ NMR²⁷ and vibrational spectra,^{28,29} all indicated that the structure consists of CB_{11}^- and $\equiv C-B^+-C \equiv$ units as primary building blocks, where the carbon atoms in the polyhedra are statistically distributed among six possible B_P positions.

Unfortunately, agreement between the various experimental and theoretical reports ends with the electron-precise $B_{12}C_3$; no consensus exists about the preferred site of substitution of carbon atoms by boron as the carbon concentration decreases. X-ray studies indeed show an expansion of the polyhedral cage with decreasing carbon concentration, indicating that carbon atoms are preferentially replaced by boron in the icosahedral subunit;^{25b,30} this is also supported by free energy (DFT) calculations.¹⁷ However, other studies based on high pressure neutron diffraction,³¹ IR/Raman spectra,³² ESR,²⁰ thermal³³ and electrical conductivities,^{21,34} etc., are explained by assuming that carbon atoms are replaced in the polyhedra only after the complete conversion of all $\equiv C-B^+-C \equiv$ chains to $\equiv B-B^+-C \equiv$. A significant number of CB_{11}^- units are conjectured to be retained even at the carbon-poor limit.

Apart from these diverse views concerning site occupancies, there are also controversies about the comparative strengths of inter-polyhedral vs. intra-polyhedral bonding, and the nature of bonding in the three atom chains. The carbon concentration dependency of longitudinal sound velocities,³⁵ the direct increase of electrical resistivity with pressure³⁶ and high pressure neutron diffraction studies³¹ of boron carbide hint that inter-icosahedral bonds are stronger than intra-icosahedral bonds (making boron carbide a so-called "Inverted Molecular Solid"), whereas the DFT interpretation of IR and Raman diffusion measurements contradicts this viewpoint.²⁹

In the case of $\equiv C-B^+-C \equiv$ chains, the shorter C-B distance (1.44 Å) was taken to be indicative of substantial π -bonding,²² which was supported by electronic structure calculations.^{16,17} However, in neutron diffraction studies, $^{11}B_C$ is reported to have a larger anisotropic thermal parameter along the direction perpendicular to the chain; severe X-ray irradiation even displaces the B_C atoms to adjacent interstitial positions (which are restored by annealing the samples at 700–900 °C or by self-healing with time), indicating a loosely bound central B_C atom that is squeezed between the two carbon atoms due to space constraints.^{13b,37,38}

Earlier conceptions

There are conflicting theories for the bonding and properties of boron carbide. Notable among the earlier conceptions was Golikova's concept,³⁹ which correlated the degree of amorphousness with the number of atoms per unit cell, as in the case of amorphous silicon and germanium. This was refuted by Werheit and co-workers; they initially hypothesized that the Jahn–Teller distortion of the icosahedra (arising from the D_{3d} symmetric environment) leads to split-off bands at the Fermi level that are mainly responsible for the properties.⁴⁰

However, in their recent reports, this hypothesis was taken back on the grounds that the computed HOMO–LUMO gap of 1.5 eV for the Jahn–Teller-distorted neutral $B_{12}H_{12}$ considerably exceeds the distance between the actual valence and the split-off band.¹⁴ Furthermore, such a split-off band, if it exists, implies extended states, while the interpretation of transport properties requires the localization of states. Recently, the same group reported, albeit qualitatively, that the valence electron deficiency arising from the reduction of carbon concentration correlates with the vacancies and anti-site defects.¹⁴

Some experimentalists endorse the bipolaron model proposed by Emin^{38,41} for explaining electronic transport in boron carbides. Based on the fact that the spin density of boron carbide is two orders of magnitude lower than the concentration of charge carriers, *i.e.*, holes, Emin proposed that the charge carriers are paired-up to form small spinless bipolarons, similar to the Cooper pairs in superconducting materials. To explain the formation of bipolarons, the model assumes that the $\equiv C-B^+-C \equiv$ chains of the ideal $B_{12}C_3$ are replaced by neutral $\equiv B-B^+-C \equiv$ chains upon carbon reduction until all the $\equiv C-B^+-C \equiv$ chains are exhausted. This substitution deprives the CB_{11} polyhedral units of their requirement for additional electrons. Emin proposed that two such neutral CB_{11} units may disproportionate: $2CB_{11} \rightarrow CB_{11}^- + CB_{11}^+$ leading to the formation of CB_{11}^+ , which is the chemical equivalent of a bipolaron. This model successfully explained several properties of boron carbide, but the implications of this model on structure and bonding are inconsistent with all the theoretical studies reported so far, and also with several other experimental reports as well.^{14,40}

Clearly, there are many questions (and models) around boron carbide. We see three as fundamental: (1) Why does boron carbide refuse to be electron-precise? (2) How does electron deficiency-induced partial occupation of the valence bands affect the chemical bonding in the material? (3) How are electron deficiency and disorder in site occupancies related? Our attempts to answer these questions also reveal how the seemingly conflicting models proposed earlier nevertheless selectively describe well some aspects of the nature of boron carbide.

We have chosen the most symmetric composition $B_{13}C_2$ and employed a deconstructive approach. The structure is broken into molecular fragments and is assembled back into sublattices, all along inquiring into the evolution of the molecular orbitals of the fragments into bands of the extended structure.

Computational methodology

Geometrical optimization of the selected molecular models are done using the Gaussian 98 suite of programs⁴² at the density functional-based B3LYP/6-31G* level of theory;⁴³ frequency calculations characterize the nature of the stationary points. For arriving at the equilibrium geometries of the extended structures, we employ the DFT-based VASP program.⁴⁴ This, together with the extended Hückel⁴⁵ (eH)-based YAEHMOP suite of programs,⁴⁶ is used for computing the band structures and density of states. We employ eH COOP⁴⁷ (Crystal Orbital Overlap Population) analysis as the primary tool for exploring

the nature of bonding. In the VASP calculations, we chose ultrasoft pseudopotentials based on the projector-augmented wave method⁴⁸ using the local density approximation,⁴⁹ which is ideal for arriving at equilibrium geometries. All these calculations are well-converged with respect to the chosen cut-off energy and k-point sampling (by the Monkhorst–Pack scheme⁵⁰). The energies of the MOs for the molecules (as well as those of the fragments) used in the interaction diagrams are derived from eH calculations.

Results and discussion

Molecular models

We start with the most symmetric $B_{12}(CBC)$ form ($B_{13}C_2$) and construct molecular models that closely simulate the bonding environment of the fragments in the boron carbide structure. Fig. 2 shows the D_{3d} symmetric bonding environment of the B_{12} and $\equiv C-B-C \equiv$ units in $B_{13}C_2$. The upper and lower triangles of B_p atoms in the B_{12} unit are connected to other distinct B_{12} units. The central six B_{eq} atoms form a distorted hexagon (resembling the chair form of cyclohexane) and are connected to $\equiv C-B-C \equiv$ units.

Modelling the B_{12} environment

It has long been suspected that the varying carbon concentration of boron carbide has an electronic origin. To see how this might happen, we analyze the nature of the MOs of B_{12} units, $\equiv C-B-C \equiv$ chains and the interactions among them. For the B_{12} unit, we ignore the 12 MOs formed by the outward-pointing sp hybrids of the boron atoms, as they are mostly involved in *exo*-polyhedral σ -bonds and should lie, as a group, lower in energy.⁵¹ Among the MOs formed from the rest of the 12 sp hybrids that point towards the center of the icosahedra and the 24 tangential p-orbitals, only the 13-most bonding MOs are filled to give B_{12}^{2-} . They transform as $a_g + t_{1u} + h_g + g_u$ in an ideal icosahedral symmetry; these are the $n + 1$ ($n = 12$) skeletal MOs of the Wade Model.⁵² Of these, the lowest a_g is of pure radial character and the HOMO, g_u , arises purely from the tangential p-orbitals. The remaining t_{1u} and h_g have substantial radial-tangential mixing.⁵³

We anticipate that the valence bands of boron carbide arise from the HOMOs (Highest Occupied Molecular Orbitals) of B_{12} units interacting either with the frontier MOs of $\equiv C-B-C \equiv$ chains or with the adjacent B_{12} units. These interactions will be predominantly of π -type because the HOMOs of the B_{12} units are mainly tangential. We have constructed two molecular models to mimic these

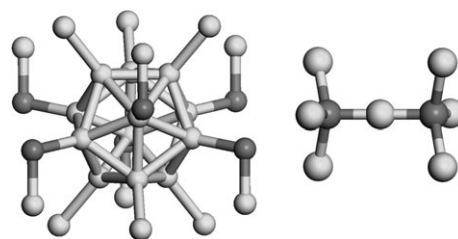


Fig. 2 The bonding environment of B_{12} units and $C-B-C$ units in $B_{13}C_2$.

π -interactions. The first model has six fluorine atoms connected to the B_{Eq} atoms, modelling $-B-C\equiv$ interactions; in the second model they are at the B_{P} positions to mimic the B_{12} units. Fluorine is selected as a substituent due to its small size and to bring into focus the π -interactions. The π -interaction will be moderate in the model, as the π -type lone pairs of fluorine are low in energy and quite contracted. In the real structure, the π -interaction may be larger.

To start, we explore the nature of these π -interactions between the B_{12} skeletal MOs (as in icosahedral $B_{12}H_{12}^{2-}$) and the fluorine substituents using eH calculations. Fig. 3 shows the perturbation of the thirteen skeletal bonding orbitals (filled) of icosahedral $B_{12}H_{12}^{2-}$ by fluorine atoms, upon axial and equatorial substitutions, leading to $B_{12}F_6H_6^{2-}$ isomers. The energies of the MOs were obtained from eH calculations using standard bond lengths close to those observed experimentally. ($B-B = 1.79$, $B-F = 1.39$ and $B-H = 1.20$ Å).

Due to the reduced D_{3d} symmetry of the substituted systems, the multi-fold degeneracies of the MOs in the icosahedral B_{12} are lost. The four-fold degenerate g_u HOMO of $B_{12}H_{12}^{2-}$ (I_h) splits into $a_{1u} + a_{2u} + e_u$ in D_{3d} . These MOs will have antibonding interactions with the appropriate combination of fluorine lone pairs. Their in-phase combinations lie low in energy, and are mostly of fluorine character due to the higher electronegativity of fluorine. However, their out-of-phase combinations, which are predominantly concentrated on the boron atoms of the polyhedron, are destabilized with respect to $B_{12}H_{12}^{2-}$. Removal of electrons from this system would result in π -bonding between the polyhedra and fluorine atoms.

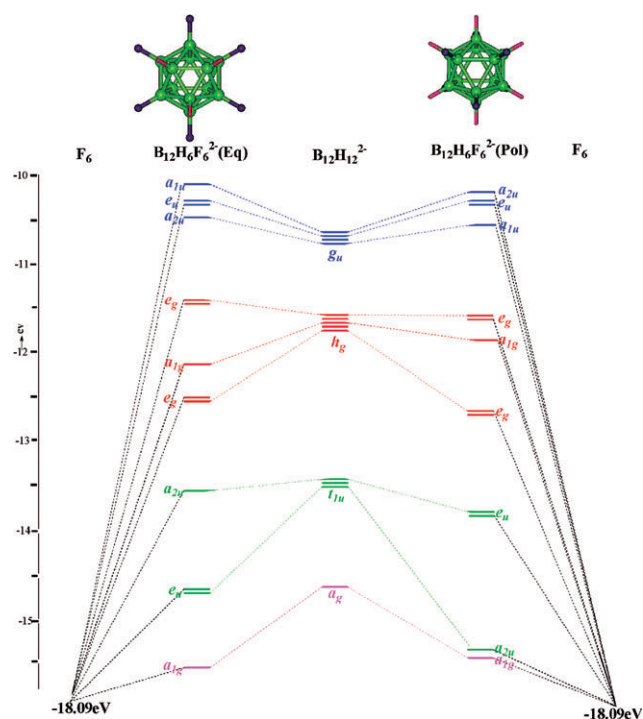


Fig. 3 The perturbation of skeletal MOs of icosahedral $B_{12}H_{12}^{2-}$ by the substitution of fluorine atoms at the equatorial and polar sites.

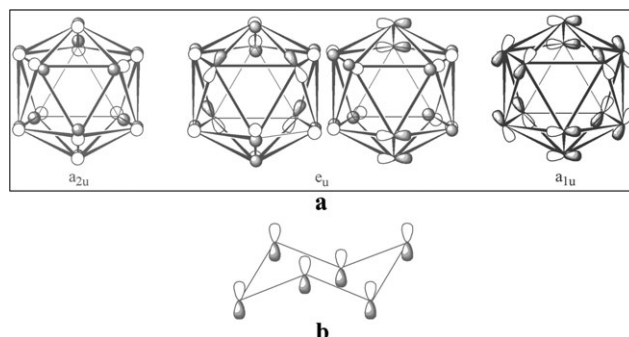


Fig. 4 (a) The D_{3d} MOs derived from the HOMO (h_g) of B_{12}^{2-} polyhedra. (b) A side view of the central hexagon fragment of the a_{2u} MO.

The splitting of the HOMO is the same for both isomers, as they belong to the same point group. However, the ordering of the levels reverses between the isomers. Since rationalization of this MO ordering is critical in determining whether B_P or B_{Eq} are involved in partial multiple bonds in the electron-deficient boron carbide, we look in detail at the nodal properties of the four MOs of the B_{12}^{2-} unit in a D_{3d} environment. Seen along the C_3 axis, they are drawn in Fig. 4.

To describe the nodal properties of these MOs, we focus separately on the top and bottom triangle of B_P atoms, and then their interactions with the central distorted hexagonal ring. The a_{2u} MO is all-bonding between the B_P atoms, while the interactions between the central B_{Eq} atoms are antibonding due to the distortion of the hexagon (as the side view of the central hexagon in Fig. 4b shows). The $B_{\text{Eq}}-B_{\text{Eq}}$ overlap in the a_{2u} MO is σ -antibonding and π -bonding; π dominating. In the case of a_{1u} , the situation is reversed. This MO is antibonding between B_P atoms, but the B_{Eq} atoms are bonding with each other. In both MOs, the interaction of the central hexagon with the triangular B_P atoms of the top and bottom is bonding; the difference is in the nature of the interaction, *i.e.*, a_{2u} has strong end-on σ -overlap while a_{1u} has π -type. The magnitude of the AO coefficients at each atom also differs substantially, depending on the nature of the interactions (not shown in the Fig. 4). In a_{2u} , the coefficients are larger for B_P atoms. On the contrary, in the a_{1u} MO, the coefficients are large on the B_{Eq} atoms. The doubly degenerate e_u MO has mixed characteristics of both of these MOs in different regions of the skeleton.

The size of the orbital coefficients allows us to understand how the substitution of six fluorine atoms at equatorial and axial positions brings about the order reversal in the splitting of the h_g set of the icosahedra. π -Interactions in fluorine substitution at the polar positions destabilize a_{1u} most, as this MO has concentrated more at the B_P positions; conversely, equatorial fluorine substitution exerts maximum destabilization on a_{2u} .

To understand how electron deficiency affects the bonding, we have removed two electrons from both of these fluorinated models and optimized the neutral $B_{12}H_6F_6$ geometries at the B3LYP/6-31G* level of theory. The calculated bond lengths of the two isomers are given in Fig. 5, along with the $B_{12}F_{12}^{2-}$ geometry for comparison. The B_{12} skeleton undergoes substantial deformation, different in nature for the isomers.

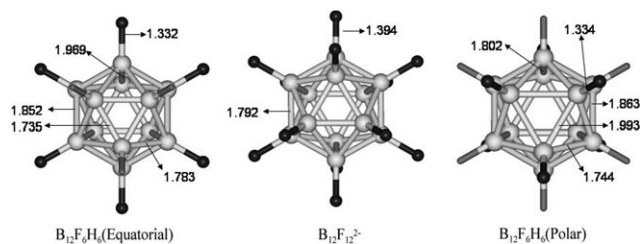


Fig. 5 DFT-optimized geometries of fluorine-substituted isomers.

Compared to the B–B bond length of 1.79 Å in the electron-precise $B_{12}F_{12}^{2-}$, the B_P – B_P distances of the equatorially-substituted neutral $B_{12}F_6H_6$ are shortened to 1.73 Å, while in the polar isomer they are elongated to 1.99 Å.

The computed LUMO of both isomers of the neutral $B_{12}H_6F_6$ (Fig. 6) shows the expected antibonding π -interactions between the B_{12} skeleton and the six fluorine atoms.

Partial B–F multiple bonding, delocalized over all the B–F bonds of the skeleton, is implied. The observed B–F distance of 1.33 Å in both isomers is shorter than the singly-bonded B–F distance (1.39 Å) computed for the electron-precise $B_{12}F_{12}^{2-}$. Since electrons are removed from a MO that is bonding within the B_{12} skeleton, the strengthening of the *exo*-B–F bonds also results in a weakening of the polyhedral B–B bonding.

Frequency calculations characterize both of these $B_{12}F_6H_6$ isomers as stationary points on their potential energy surface; so perhaps these molecules can be made. Substitution of chlorine atoms in place of fluorine atoms also gives similar results.

The ability of B_{12} units to engage in *exo*-polyhedral multiple bonding has been suggested in recent work.^{54–57} In our earlier theoretical studies on polyhedral boranes, we have shown that the polyhedral cages can shed two or more electrons, even with two electronegative substituents such as O, N–H, S, *etc.*⁵⁶ Further evidence for their easy oxidation comes from experimental studies on persubstituted systems.^{54,57} Hawthorne *et al.* have shown that $B_{12}(OCH_2Ph)_{12}^{2-}$ readily loses its extra two electrons, and the symmetry of the B_{12} cage is lowered from I_h to D_{3d} due to Jahn–Teller distortion,⁵⁴ similar to the geometry of the equatorial $B_{12}F_6H_6$ isomer.

Returning to the consequences for the boron carbide problem, the results from the two molecular models indicate that electron deficiency in boron carbide (due to the decrease in

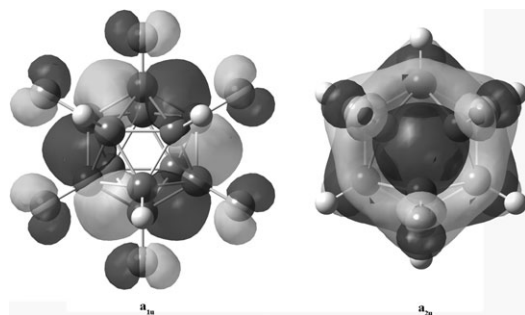


Fig. 6 The LUMO of equatorial and polar isomers of the neutral $B_{12}F_6H_6$ obtained from DFT calculations.

carbon concentration) may lead to exohedral π -bonding between adjacent B_{12} units at the B_P sites, or between the B_{12} unit and the $\equiv C-B-C \equiv$ chains at the B_{Eq} sites. This would lead to strong *exo*-polyhedral bonds at the expense of polyhedral bonding. These $B_{12}F_6H_6$ isomers might serve as realistic chemical models of bipolarons, formed by the *exo*-multiple bonded B_{12} units in boron carbide, models that perhaps are chemically more meaningful than the controversial CB_{11}^+ polyhedra predicted earlier.³⁸ In the next section, we inquire how electron deficiency affects the nature of bonding in the three-atom chains.

Modelling the CBC environment

As described earlier, each carbon atom of the linear $\equiv C-B^+-C \equiv$ chain is surrounded by three B_{12} units in a staggered orientation, forming a D_{3d} symmetric environment. To retain the important nonbonding π -interactions between the B_{12} units and the C–B–C chains, we now model the B_{12} units by fluorine atoms. This leads us to a $F_3C-B^+-CF_3$ molecular model.

The MOs of D_{3d} $F_3C-B^+-CF_3$ can be constructed in a number of ways, either from the interaction of CB^+C units and 6 F atoms or from two CF_3 radicals and a B^+ . The latter approach is more informative and is shown in Fig. 7.

The C–B distances are kept at 1.44 Å (as observed in the experimental $B_{13}C_2$ structure) and the C–F distances are kept at a standard 1.30 Å. The two HOMOs of $F_3C-B^+-CF_3$ are of a_{1g} and a_{2u} symmetry, and are C–B bonding but B–F

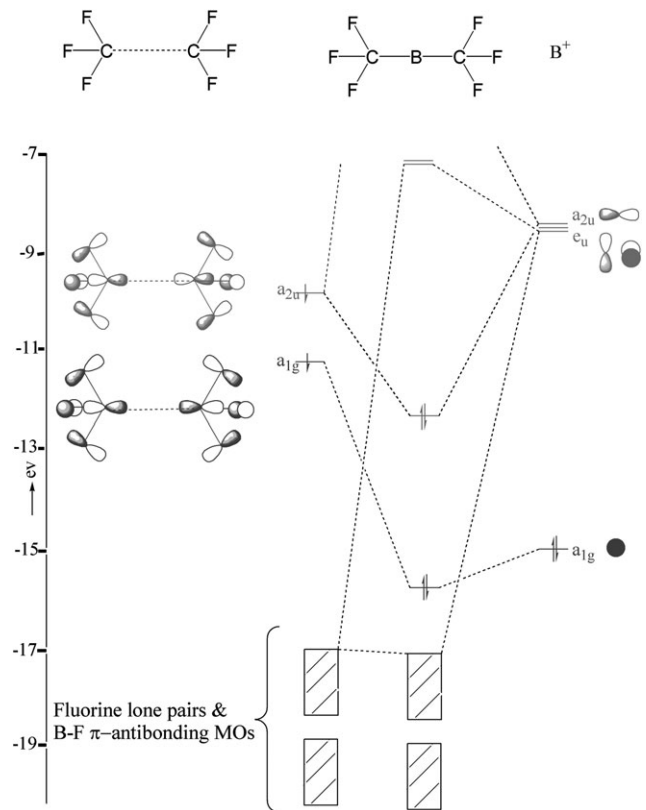


Fig. 7 The interaction diagram between the two CF_3 fragments (left) with the central boron cation (B^+ , right), resulting in the C–B σ -bonding.

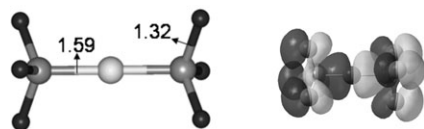


Fig. 8 The DFT-optimized geometry of BC_2F_6^+ and its HOMO.

π -antibonding, with some B–F σ -bonding as well. Electron deficiency will result in the removal of electrons from the a_{2u} MO; as a result, the C–B σ -bonds will be weakened, but there will be slight π -bonding between the carbon and fluorine atoms.

The computed Mulliken overlap population (OP) value in BC_2F_6^+ is 0.77 for C–B and 0.51 for C–F bonds by eH calculations. After the removal of two electrons ($\text{BC}_2\text{F}_6^{3+}$), the OP changes to 0.42 for the C–B bonds and 0.56 for the C–F bonds. The effects seen are those expected.

Fig. 8 shows the optimized geometry of the $\text{F}_3\text{C}-\text{B}^+-\text{CF}_3$ molecule at a B3LYP/6-31G* level of theory, along with the shape of the a_{2u} HOMO. The computed C–B distance of 1.59 Å is longer than the C–B bond length of 1.44 Å observed in boron carbide. Assuming that the elongation of C–B bonds in our model is due to pronounced destabilizing π -interactions from the fluorine atoms, we replaced the fluorine atoms by hydrogens, where such interactions are completely absent. The optimized geometry of $\text{H}_3\text{C}-\text{B}^+-\text{CH}_3$ has a C–B distance of 1.48 Å, still somewhat longer than the observed 1.44 Å in boron carbide.

Frequency calculations indicate that $\text{F}_3\text{C}-\text{B}^+-\text{CF}_3$ is a minimum on the potential energy surface. However, the geometry optimization of this molecule after removing two more electrons fails to converge; both CF_3 fragments are completely detached from the central boron atom.

It is clear that electron deficiency lengthens the C–B–C chain. It has been suggested that the 1.44 Å C–B distance in boron carbide is shortened as a consequence of “squeezing” of the $\text{C}-\text{B}^+-\text{C}$ chain by the constraints of its bonding to the B_{12} icosahedra.³⁸ The observed flattening of the carbon tetrahedra (bond angles $\text{B}_{\text{Eq}}-\text{C}-\text{B}_{\text{Eq}} = 117^\circ$ and $\text{B}_{\text{C}}-\text{C}-\text{B}_{\text{Eq}} = 99^\circ$) in the experimental structure of boron carbide also supports this viewpoint.¹³ However, such “squeezing” of single bonds is rare elsewhere in chemistry⁵⁸ and we are loathed to accept it here. It is possible that the short $\text{B}_{\text{C}}-\text{C}$ distance is a result of crystallographic disorder of the type indicated schematically in Fig. 9 below. Since there are six such crystallographically-equivalent positions in the local D_{3d} symmetry of the CBC chain, this disorder may be the cause of the large thermal ellipsoids observed in the diffraction studies.¹³

In one X-ray structural study of a boron-rich boron carbide, it was reported that a quarter of the C–B–C chains were replaced by a B_4 ring incorporating two of the six B atoms in Fig. 9, together with the two C atoms, replaced by B.^{37b} To bend $\text{CF}_3-\text{B}^+-\text{CF}_3$ from 180° to 150° takes only 7.5 kcal mol^{−1}.

In the next section we investigate the nature of the interactions between the various fragments in boron carbide by eH calculations.

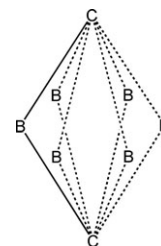


Fig. 9 A disorder that is possibly responsible for the short B–C distance in the C–B–C unit. The displacement has been exaggerated for clarity.

Fitting the fragments together: conflicting conclusions

So far, our MO analysis, using $\text{B}_{12}\text{F}_6\text{H}_6$ isomers as models, indicates that electron deficiency in boron carbide may lead to *exo*-polyhedral multiple bonding, either between two adjacent B_{12} units or between B_{12} units and CBC chains. Our $\text{F}_3\text{C}-\text{B}^+-\text{CF}_3$ model implied that *exo*-polyhedral multiple bonding is likely between B_{12} and CBC units. Combining these two results, it seems likely that such partial multiple bonding is at work between B_{12} and CBC units. What would be needed is for the HOMOs of these two fragments to interact and the electrons to be removed from the resulting antibonding combination. But do these fragment frontier MOs have appropriate symmetry to interact?

To answer this question, we use another simple molecular model, one which simulates the interaction between the C–B–C chains and the B_{12} units. Fig. 10 depicts the bonding environment around the carbon atom, which is the nerve center for the formation of *exo*-polyhedral multiple bonds. The simplest model of this environment is $\text{HC}(\text{BH})_3$, where the $-\text{B}_{12}$ units are replaced by $[-\text{B}-\text{H}]$ groups and where $\equiv\text{C}-\text{B}^+-\text{C}\equiv$ is replaced by a C–H bond. Since the a_{1u} and a_{2u} frontier MOs of the B_{12} units are filled, tangential π -orbitals, modelling of the B_{12} units requires charged $[-\text{B}-\text{H}]^{3-}$ groups, where the two unhybridized p-orbitals of the boron atom are filled. Therefore, the net charge of the model molecule will be $\text{HC}(\text{BH})_3^{9-}$.

We need, thus, the orbitals of $\text{HC}(\text{BH})_3^{9-}$, which may be constructed from CH and $[\text{BH}]_3^{9-}$. For the $[\text{BH}]_3^{9-}$ fragment, the MOs arising from the three inward-pointing sp hybrids and two sets of tangential p-orbitals form nine MOs, drawn schematically in Fig. 11. The MOs constructed from the tangential (Fig. 11a) and π -type (Fig. 11b) p-orbitals simulate the two different frontier MOs, a_{1u} and a_{2u} , of the B_{12} unit, respectively, and have to be filled. The three radial MOs then contain the three electrons left (Fig. 11c), and are set up to form the C–B σ -bonds upon interaction with the C–H unit. From our knowledge of main group overlapping, we reason that the splitting of energy levels will be most pronounced in the radial set, followed by the tangential orbitals, while the π -set should have the smallest splitting in the group.

The interaction between this $[-\text{B}-\text{H}]_3^{9-}$ fragment and the C–H group in a C_{3v} environment is illustrated in Fig. 12. The C–B bond lengths are kept at 1.60 Å, as reported in the X-ray structure of B_{13}C_2 . All the MOs shown in the diagram for $\text{HC}(\text{BH})_3^{9-}$ are filled. The HOMO of this molecule, a_2 ,

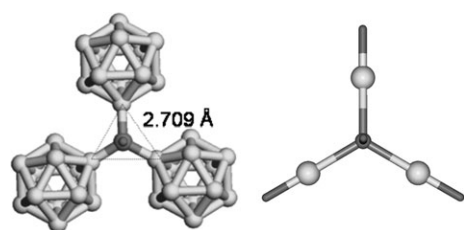


Fig. 10 The bonding environment of carbon in boron carbide and its molecular model $\text{HC}(\text{BH})_3^{9-}$.

corresponds to the most antibonding combination of in-plane tangential p-orbitals of the three boron atoms. None of the MOs of the C–H fragment has a_2 symmetry; hence, this MO remains nonbonding. This implies that removal of electrons from this MO will not lead to *exo*-polyhedral multiple bonding. Despite it having no interactions with the central C–H group, this MO is the HOMO of the molecule, indicating that the antibonding interactions between non-bonded boron atoms are not insignificant, even when they are separated by 2.70 Å. The overlap of one tangential p-orbital with the other two at this distance is computed to be 0.19 by eH calculations.

Note that the a_2 MO of the $\text{HC}(\text{BH})_3^{9-}$ model simulates the out-of-phase combination of the three a_{1u} MOs from the B_{12} units around the carbon. Similarly, the a_1 MO in the $\text{HC}(\text{BH})_3^{9-}$ model simulates the most bonding combination of the three a_{2u} MOs of the B_{12} units around the carbon. In boron carbide, the interaction of the tangential set (Fig. 11b) will be even more pronounced because in the a_{1u} MO of B_{12} units there are bigger coefficients at B_{Eq} than in the π -type MOs (Fig. 11a), which lead to the a_{2u} orbitals of the polyhedra. Hence, it is very unlikely that the antibonding combination of a_{2u} MOs with carbon will rise above their a_{1u} counterparts in the extended boron carbide structure. This implies that if a unique ‘split-off’ valence band exists in boron carbide (as we suggested earlier), it will be made up from a_{1u} -type B_{12} orbitals rather than a_{2u} -type. To find out what actually happens, we have looked at the 2D lattice.

Interactions in a 2D B_{12}C_2 lattice

We next construct a 2D model, one that has a layer of B_{12}H_6 units connected through C–H groups. As shown in Fig. 13, the model is a hexagonal lattice that has one B_{12} and two $\text{HC}\equiv$ units in its primitive cell. To be electron-precise, this model requires two electrons per unit cell.

The band structure for this 2D polymer is obtained from eH calculations, using components of the experimental geometry of the B_{13}C_2 structure,¹³ and is given in Fig. 14. The colors of

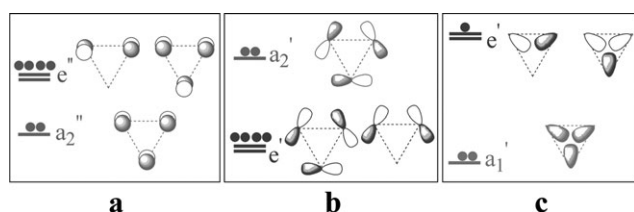


Fig. 11 A schematic illustration of the MOs generated by (a) π tangential and (c) radial sp hybrids of a D_{3d} $[\text{BH}]_9^{9-}$ fragment.

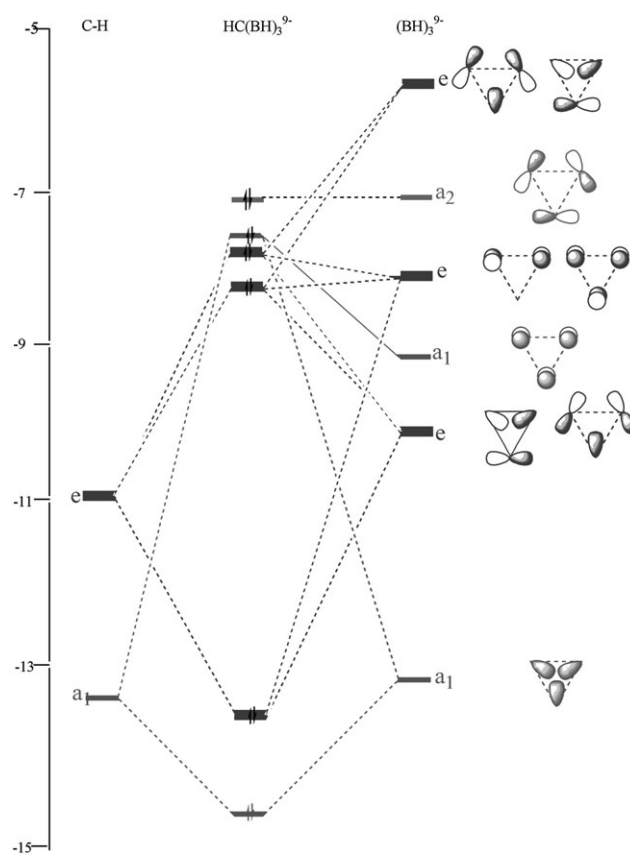


Fig. 12 Interaction of MOs between the $(\text{BH})_3^{9-}$ fragment (C_{3v}) with a CH group at the center. MOs of dissimilar symmetry are shown in distinct colors.

the bands follow that of the B_{12} MOs in Fig. 3; the bands are assigned with an assumption that, at G (Brillouin zone center, Γ), the energy level pattern of the B_{12} unit in the extended network is similar to that at the molecular level. The valence band structure of $\text{B}_{12}\text{H}_6(\text{CH})_2^{2-}$ exhibits a series of almost flat energy bands, with little variation in energy; this is a sign of localization. There is a band gap (~ 5.3 eV) at 54 electrons, *i.e.*, a -2 charge.

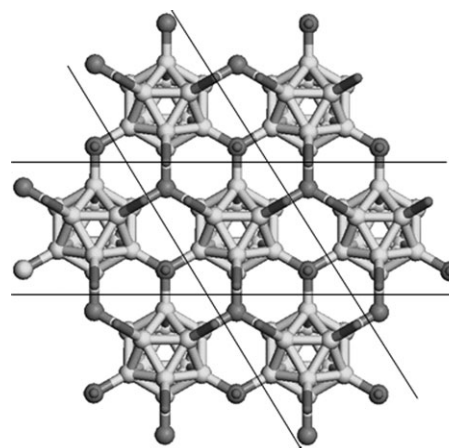


Fig. 13 The structure of a 2D model $\text{B}_{12}\text{H}_6(\text{CH})_2$.

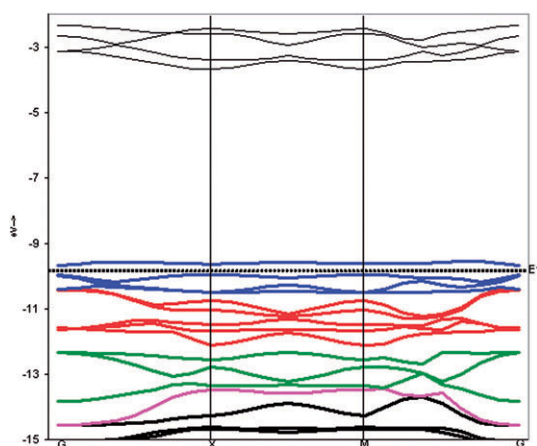


Fig. 14 The band structure of the 2D polymer $B_{12}H_6(CH)_2$.

As we outlined above, our interest is in electron-deficient structures relative to this electron count. At the top of the valence band is a band very slightly split-off (by ~ 0.23 eV) from the other bands. This band would be vacated in electron-deficient neutral $B_{12}H_{10}(CH)_2$. The COOP curves (Fig. 15) indicate that in this band, there is intra-polyhedral $B_{Eq}-B_{Eq}$ bonding; there is also B_P-B_{Eq} bonding and some B_P-B_P antibonding. As we have seen earlier, these features— B_P-B_P antibonding and $B_{Eq}-B_{Eq}$ bonding—are characteristic of the a_{1u} HOMO of the B_{12} unit (Fig. 4 and Fig. 6). This suggests that the top band arises from this MO.

We anticipated that this high-lying MO should be nonbonding with the C–H group modelling CBC (see previous discussion), as discussed above. Surprisingly, however, the COOP curve shows the split-off band to be $B_{Eq}-C$ bonding. This is possibly due to mixing-in of some antibonding B_{12} MOs. The implication is that the $B_{Eq}-C$ bond will be weakened by the removal of electrons from the electron-precise composition, in

contradiction to our expectations of $B_{Eq}-C$ antibonding in this band. Indeed, the $B_{Eq}-C$ curve shows some antibonding character, but this occurs below the Fermi level of the neutral $B_{12}H_6(CH)_2$. Only intrapolyhedral B_P-B_P bonds will be strengthened by removing electrons from the electron-precise compound. The COOP between the B_{Eq} atoms of the adjacent B_{12} units (dotted line in Fig. 15) shows that in this region of energy, there is significant antibonding character between these atoms, even though they are 2.7 Å apart.

We wondered if replacement of the $\equiv C-B^+-C \equiv$ chains by a simple C–H group in the model 2D polymer might be the reason why $B_{Eq}-C$ antibonding emerges well below the Fermi level. Hence, we did another calculation, replacing the C–H groups with $\equiv C-B^+-CH_3$ groups in the model structure. However, the valence band structure and the nature of the COOP curves (not shown here) remain mostly unchanged. While these models are instructive, it is clear that their description of the bonding in boron carbide is not complete.

Bulk calculations on boron carbide

The range of carbon concentrations in boron carbide can be ideally viewed as being between $B_{12}C_3$ and $B_{14}C$; as many as two carbon atoms are replaced by boron atoms (though both extremes of this variation are not experimentally characterized). This amounts to a total variation of two electrons per rhombohedral unit cell. Hence, we chose the most symmetric $B_{13}C_2$ ($B_{12}CBC$) composition and studied the effect on its bonding of adding or removing one electron from the unit cell. The addition of one electron, *i.e.*, $B_{13}C_2^{-1}$, simulates the electron-precise $B_{12}C_3$ composition, while removing one electron, as in $B_{13}C_2^{+1}$, simulates the carbon poor extreme of $B_{14}C$. Structural optimization of these charged unit cell models permit the studying of the electronic variation with full preservation of lattice symmetry.

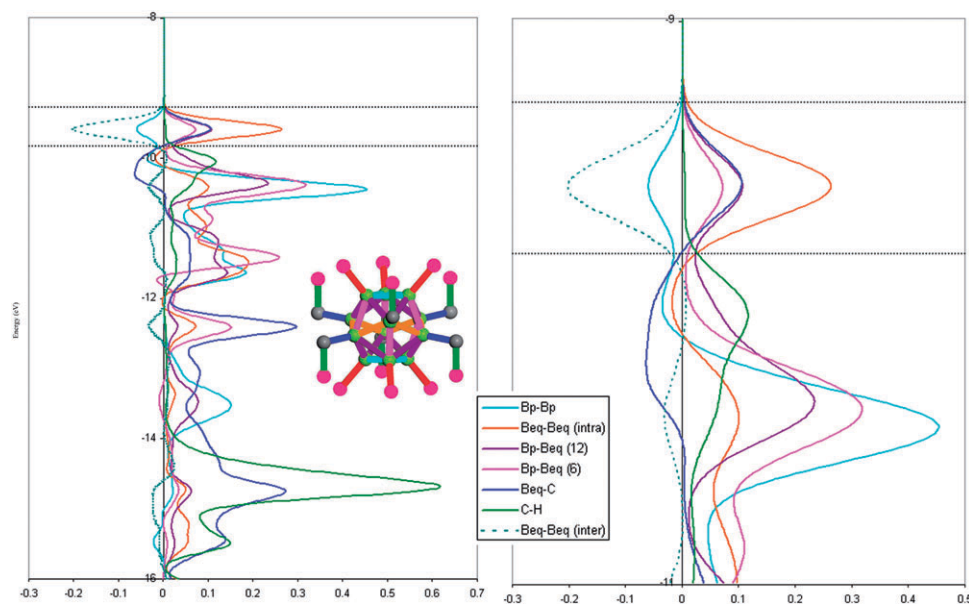
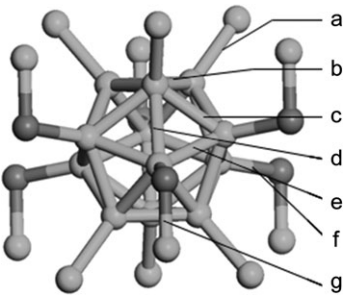


Fig. 15 (a) COOP curves for various bonds in $B_{12}H_6(CH)_2$. Different types of bonds and their COOP curves are shown in distinct colors. (b) An enlarged view of the COOP curves around the Fermi.

Table 1 Optimized geometric parameters (distances in Å, angles in °) of boron carbide from DFT calculations


Parameter	$B_{13}C_2^{-1}$	$B_{13}C_2$	$B_{13}C_2^{+1}$	Variation ^a	Adjusted variation ^b
Cell length (<i>a</i>)	5.26	5.13	4.99	−0.27	
Rhombohedral angle	65.19	66.08	67.29	+2.1	
a	1.77	1.75	1.70	−0.07	−0.01
b	1.82	1.76	1.72	−0.10	−0.04
c	1.81	1.80	1.78	−0.03	+0.03
d	1.81	1.77	1.75	−0.06	0.00
e	1.77	1.77	1.76	−0.01	+0.05
f	1.64	1.59	1.54	−0.10	−0.04
g	1.44	1.43	1.43	−0.01	+0.05
$B_{Eq}-C-B_{Eq}$	116.56	117.3	118.35		
$B_{Eq}-C-B_c$	100.82	99.57	97.44		

^a For two electrons. ^b Variation +0.06 Å. See text for explanation.

In our study of $B_{13}C_2$ with +1, 0 and −1 charges, we used a plane-wave cut-off energy of 500 eV with a k-point separation of about 0.027 \AA^{-1} ($8 \times 8 \times 8$ mesh). Since boron carbide is reported to have negligible spin density over its range of carbon substitution, we chose to do all the calculations without spin polarization. The results of the geometry optimization are given in Table 1. The optimized geometric parameters of $B_{13}C_2$ are comparable to experimental reports. We did not do a direct comparison between experimental and computed structural parameters since, in all the experimental reports, there is ambiguity about the carbon concentration and mixed occupancies.

Boron carbides of varying carbon concentration (*i.e.*, the carbon-rich $B_{12}C_3$, the high symmetric $B_{13}C_2$ and the boron-rich $B_{14}C$) are modelled by anionic $B_{13}C_2^{1-}$, neutral $B_{13}C_2$ and cationic $B_{12}C_3^{1+}$, respectively. Ideally, geometry optimization of these model systems should reveal the strengthening and weakening of different bonds with increasing carbon concentration, *i.e.*, weakened bonds will be elongated and strengthened bonds will be shortened. However, due to the difference in total molecular charge for the same atomic composition ($B_{13}C_2^{1+}$, $B_{13}C_2$, $B_{13}C_2^{1-}$), the unit cell expands with the addition of more electrons, elongating all the bonds. However, the variation in bond angles around carbon still remains a good indicator of changes in the bonding environment. As we move from $B_{13}C_2^{1-}$ to $B_{13}C_2^{1+}$, the ideally sp^3 -hybridized carbon tends to be sp^2 -hybridized. The $B_{Eq}-C-B_{Eq}$ bond angle increases from 116.56° in $B_{13}C_2^{1-}$ to 118.35° in $B_{13}C_2^{1+}$, whereas the $B_{Eq}-C-B_c$ bond angle is reduced from 100.82° to 97.44° . This clearly indicates the formation of multiple bonding between B_{Eq} and C, and the weakening of the σ -bond between C and B_c .

To compare the bond distances, we computed (see the last column of Table 1) an “adjusted variation” by adding 0.06 \AA (the average effect on every bond of subtracting two electrons). Judging by the adjusted variation, on moving from the electron-precise $B_{13}C_2^{1-}$ to the electron-deficient $B_{13}C_2^{1+}$, the *exo*-polyhedral $C-B_{Eq}$ bonds should be shortened by 0.04 \AA , while the $C-B_c$ bond length of the $C-B-C$ chains should elongate by 0.05 \AA , indicative of bond weakening. The *exo* B_P-B_P bonds are also compressed by 0.01 \AA , though this is not as pronounced as for $B_{Eq}-C$. These trends also indicate that *exo*-polyhedral multiple bonding is indeed present, formed preferentially between $B_{Eq}-C$ rather than B_P-B_P . Within the polyhedra, the maximum adjusted variation (-0.04 \AA) is observed between B_P-B_P bonds, as in the case of our model calculations with $B_{12}F_6H_6$. Since the removal of electrons leads to the shortening of this bond, this case appears to be related to the equatorial isomer of $B_{12}F_6H_6$ —another indication that *exo*-polyhedral multiple bonds are preferentially formed at the equatorial sites ($B_{Eq}-C$). However, the trend in the $B-B$ bond length variations observed in our molecular models is not exactly reflected in the extended structure calculations. This may be due to the increased constraints of the translational symmetry in boron carbide, absent in the molecular models, which have more degrees of freedom to relax their bond lengths. Or it may just be that the bonding in boron carbide is more complex than what is expected from the simple molecular models discussed earlier.

We have also analyzed the Crystal Orbital Overlap Population (COOP) curves generated from eH calculations on the DFT-optimized structure of $B_{13}C_2$. The different types of bonds in $B_{13}C_2$ and their COOP curves are given in Fig. 16.

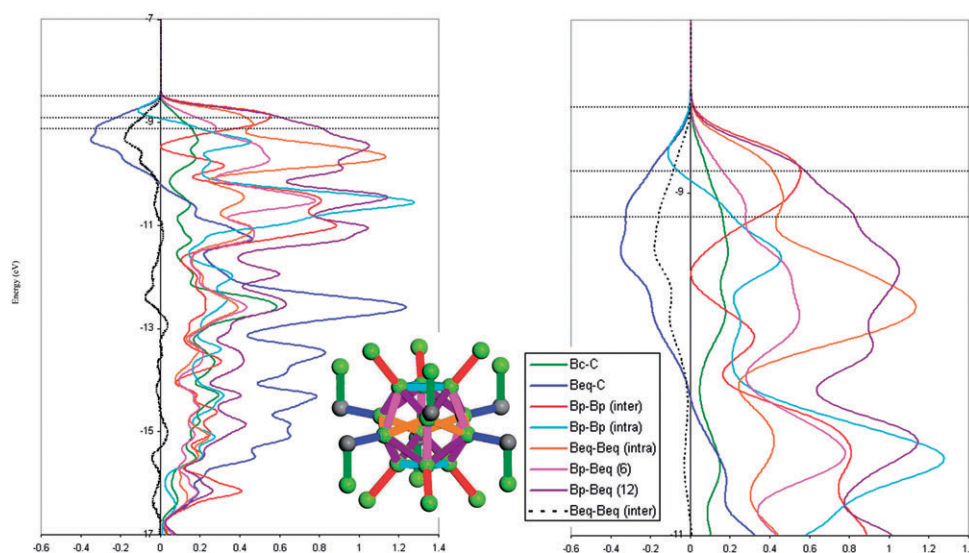


Fig. 16 COOP curves for the various bonds in boron carbide. Different bonds and their corresponding COOP curves are colored uniquely. The interaction between the B_{Eq} atoms of adjacent B_{12} units is shown in dotted lines. The close-up picture around the Fermi is shown in a separate window.

The COOP curves for all the bonds, except $C-B_{Eq}$ and intrapolyhedral $Bp-Bp$ bonds, are bonding throughout the window shown, up to the Fermi level of $B_{13}C_2^{-1}$. However, near the Fermi level, unlike the case of the model 2D polymer, the COOP curve for $B_{Eq}-C$ shows significant antibonding character. Hence, moving from electron-precise $B_{13}C_2^{-1}$ towards electron-poor $B_{13}C_2^{+1}$ results in *exo*-polyhedral multiple bonding at B_{Eq} sites, while some of the polyhedral bonds are weakened.

The band structure of $B_{13}C_2$, computed from DFT calculations, is given, along with the eH bands, in Fig. 17. Calculations for the boron carbide system with one electron less or more are identical to the eH method, and not that different from each other by DFT. This is why we show only the calculation for the neutral species, corresponding to the middle of the three Fermi levels shown.

While the electron-precise $B_{13}C_2^{-1}$ is a semiconductor, $B_{13}C_2$ and $B_{13}C_2^{+1}$ are metallic, as expected. The DFT band structures appear very similar to the bands obtained from eH calculations, which supports the close fit of the default eH parameters with the DFT results. Unlike the case of the band structure of the 2D model $B_{12}H_6(CH)_2$, there is no split-off band at the Fermi level for the electron-deficient $B_{13}C_2^{+1}$.

Inspection of the eigenvalues at Γ show that only the top two bands are truly degenerate. We believe that these two bands arise primarily from the out-of-phase combination of the e_u MO of the B_{12} unit with the carbon atoms of the surrounding $C-B-C$ chains. Recall that this degenerate e_u set has mixed characteristics of MOs a_{1u} and a_{2u} of the B_{12} unit, and is completely missing in our simplistic $HC(BH)_3^{9-}$ model. This is the reason why the molecular models lead to ambiguous conclusions when considered separately. There is evidence of *exo*-polyhedral multiple bonding between B_{12} units and $C-B-C$ chains elsewhere in the Brillouin zone.

Disorder and semiconductivity

Putting together all the pieces of partial information from various molecular models of the idealized system, we can now investigate the origins of disorder and the semiconducting properties of samples of varying carbon concentration. The analysis of bonding in the idealized, most symmetric, form of boron carbide clearly shows that the deficiency of electrons is encouraged by the antibonding character between the B_{12} units and $C-B-C$ chains near the Fermi level. The higher stability of carbon-deficient $B_{13}C_2$ over the electron-precise $B_{12}C_3$ can be justified on this basis.

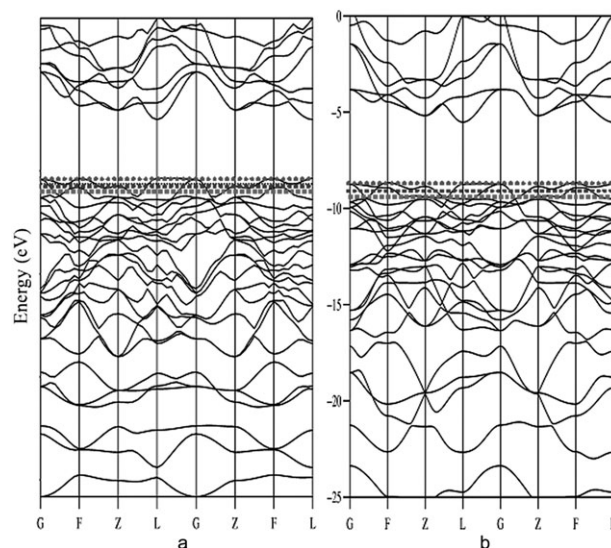


Fig. 17 The band structures of $B_{13}C_2$ from (a) DFT and (b) eH calculations. Since the band structure of the charged $B_{13}C_2^{-1}$ and $B_{13}C_2^{+1}$ are nearly identical, their corresponding Fermi levels are shown as dotted lines on the same plot.

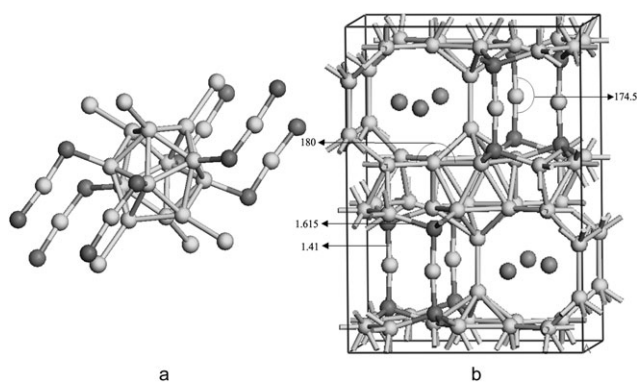


Fig. 18 (a) The bonding environment around B₁₂ and (b) the unit cell of LiB₁₃C₂.

However, even at the B₁₃C₂ composition, the removal of one electron does not completely remove the antibonding between the B₁₂ and C–B–C chain substructures. The COOP curves (Fig. 16) show that a significant amount of antibonding character between B_p and C is retained. Since electrons can only be removed by replacing carbon with boron in boron carbide, further reduction must involve the replacement of carbon atoms in the C–B–C chains, which is what led to the antibonding interactions in the first place. To escape from this internal conflict, the boron carbide structure resorts to disorder, particularly at the carbon sites. The replacement of carbon atoms by boron in the C–B–C chains is also energetically unfavorable for *exo*-σ-bonds, because of the greater bond strength of C–B vs. B–B bonds. So, for any boron carbide sample, partial replacement of carbon by boron atoms leads to disorder. B/C disorder is also stabilizing for entropic reasons. As this disorder leads to the localization of electronic states,¹⁴ boron carbide remains a semiconductor, even when the carbon concentration is varied significantly.

Structure and bonding in LiB₁₃C₂

LiB₁₃C₂ crystallizes in an orthorhombic unit cell with the space group *Imma*, and the covalent network is isomeric to B₄C, comprising the same B₁₂ and C–B–C units. The Li ions

occupy the voids, donating the electrons required by the covalent network. However, the B₁₂ unit in LiB₁₃C₂ is less symmetric when compared to B₄C as it has three distinct boron atoms. While the six B_{Eq} atoms remain the same, the six B_p atoms form two groups—four of them, which we call strained borons (B_S), are distinct from the other two (B_A). As in B₄C, B_{Eq} atoms are bonded to the C–B–C chains while B_S and B_A are involved in inter-linkages with other B₁₂ units. The difference between B_S and B_A lies in that the *exo*-bonded B atom makes an angle of 154.6° with the centroid (X–B_S–B_S), while it is almost linear in the case of B_A (X–B_A–B_A 176.8°). Another marked difference from B₄C is in the inclination of the C–B–C chains towards the B₁₂ unit. While in B₄C, the B_{Eq}–C–B_C angle tends to be perpendicular (99.6°), in LiB₁₃C₂ it has an average value of 107.9°. This is facilitated by a bending of the B_C atoms (C–B_C–C 174.8°) in LiB₁₃C₂, which is perfectly linear in B₄C. Hence, the carbon atoms are closer to sp³ hybridization, with an average angle around the B₁₂s of 110.5° (B_{Eq}–C–B_{Eq}). The bonding environment around B₁₂ and its extension in a 3D lattice is shown in Fig. 18.

Fig. 18(a) gives the bonding environment around B₁₂, which is identical to that in B₄C. However the layer structure of the B₁₂ units can be perceived in a somewhat different way, owing to the tilting of C–B–C bonds. Thus, as shown in Fig. 18(b), different B₁₂ layers are connected through the B_A–B_A bond, and the bonding within the layer comes from B_S, in addition to the common C–B–C chains.

An eH-based band structure and the COOP of some important bonds in the B/C sub lattice of LiB₁₃C₂ is given in Fig. 19. Like in B₄C, the B_{Eq}–C bond is antibonding just below the Fermi level. A VASP calculation is done on the neutral system with Li ions removed, which will be then isomorphic and isoelectronic to the existing B₁₃C₂. It is found to be less stable than B₁₃C₂ by 25.6 kcal mol^{−1} per formula unit. Optimization of LiB₁₃C₂ by a negative charge instead of an Li ion, *i.e.*, B₁₃C₂^{1−} (isoelectronic to B₁₃C₂^{1−} discussed earlier), dissociates the structure. Li seems to be vital in stabilizing the B/C covalent network intact. Presumably the covalent network in boron carbide is stronger than that of LiB₁₃C₂, irrespective of the electronic variations.

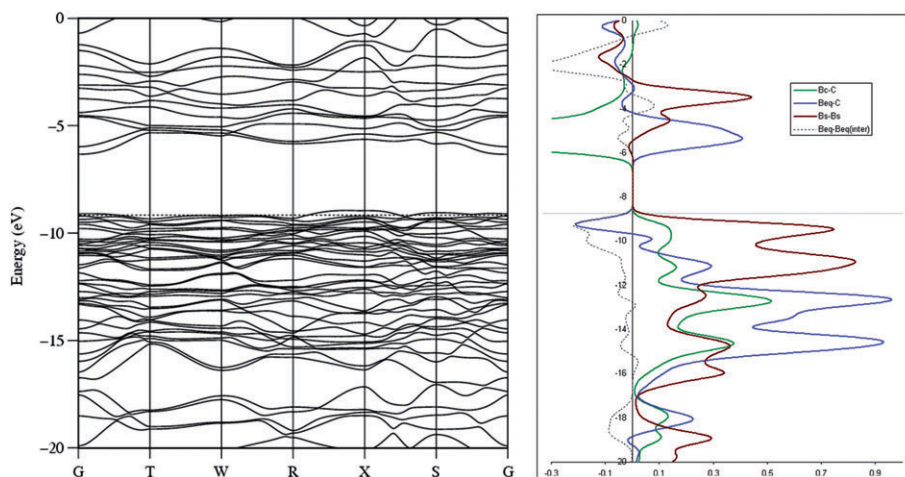


Fig. 19 The band structure and COOP curves of B/C sub lattice in LiB₁₃C₂. The COOPs of various bonds are colored differently.

Conclusion

A detailed quantum chemical investigation of the structure and bonding in boron carbide has been presented. In electron-precise boron carbide ($B_{12}C_3$), the frontier bands are characterized by significant π -antibonding interactions between the $B_{Eq}-C$ atoms, and also around the inter-polyhedral $B_{Eq}-B_{Eq}$ region. This leads to instability, for which the system tries to compensate by decreasing the carbon concentration. Hence, in different samples of boron carbide, the carbon concentration varies significantly. Removal of electrons results in strong *exo*-polyhedral $B_{Eq}-C$ bonds, but also weakens the polyhedral bonds and σ -bonds of the $C-B-C$ chains. We think that the semiconducting behavior of boron carbide over its range of carbon compositions is due to carbon substitutional disorder, which in turn leads to localized states. The seemingly mysterious experimental observations of the properties and structure of boron carbide can be understood and interpreted from this viewpoint. Our calculations show that the bonding in the B/C covalent network is stronger in boron carbide than in the electron-precise boron carbide network that has been realized in $LiB_{13}C_2$.

Acknowledgements

We are grateful to the National Science Foundation for its support of the research at Cornell through grant CHE-0204841.

References

- 1 I. J. McColm, *Ceramic Hardness*, Plenum Press, New York, 1990.
- 2 R. R. Ridgway, *J. Electrochem. Soc.*, 1934, **66**, 117.
- 3 (a) A. Lipp and K. Schwetz, *Ber. Dtsch. Keram. Ges.*, 1975, **52**, 335; (b) H. Werheit, A. Leithe-Jasper, T. Tanaka, H. W. Rotter and K. A. Schwetz, *J. Solid State Chem.*, 2004, **177**, 575.
- 4 (a) R. Telle, in *Structure and Properties of Ceramics*, ed. M. V. Swain, Materials Science and Technology, vol. **11**, VCH, Weinheim, 1994, pp. 173–266; (b) R. Telle, *Chem. Unserer Zeit*, 1988, **22**, 93.
- 5 W. Jeitschko and R. P. R.-D. Hoffmann, in *Handbook of Ceramic Materials*, ed. R. Riedel, Wiley-VCH, New York, 2000, pp. 3–40.
- 6 K. A. Schwetz and A. Lipp, Boron Carbide, Boron Nitride and Metal Borides, in *Ullmann's Encyclopedia of Industrial Chemistry*, Verlag Chemie, Weinheim, 1985, pp. 295.
- 7 H. Werheit, *Mater. Sci. Eng., B*, 1995, **29**, 228.
- 8 S. D. Hwang, D. Byun, N. J. Janno and P. A. Dowben, *Appl. Phys. Lett.*, 1996, **68**, 1495.
- 9 M. Calendra, N. Vast and F. Mauri, *Condensed Matter*, Los Alamos National Laboratory Preprint Archive, 2003, <http://xxx.lanl.gov/pdf/cond-mat/0312200>.
- 10 D. Emin and T. L. Aselage, *J. Appl. Phys.*, 2005, **95**, 013529.
- 11 N. Vojteer and H. Hillebrecht, *Angew. Chem., Int. Ed.*, 2006, **45**, 165.
- 12 D. Gosset and M. Colin, *J. Nucl. Mater.*, 1991, **183**, 161.
- 13 (a) U. Kuhlmann, H. Werheit and K. A. Schwetz, *J. Alloys Compd.*, 1992, **189**, 249; (b) G. H. Kwei and B. Morosin, *J. Phys. Chem.*, 1996, **100**, 8031.
- 14 (a) R. Schmechel and H. Werheit, *J. Phys.: Condens. Matter*, 1999, **11**, 6803; (b) R. Schmechel and H. Werheit, *J. Solid State Chem.*, 2000, **154**, 61.
- 15 H. C. Longuet-Higgins and M. de V. Roberts, *Proc. R. Soc. London, Ser. A*, 1955, **230**, 110.
- 16 D. M. Bylander, L. Kleinman and S. Lee, *Phys. Rev. B: Condens. Matter*, 1990, **42**, 1394.
- 17 (a) D. M. Bylander and L. Kleinman, *Phys. Rev. B: Condens. Matter*, 1991, **43**, 1487; (b) S. Lee, D. M. Bylander, S. W. Kim and L. Kleinman, *Phys. Rev. B: Condens. Matter*, 1992, **45**, 3248.
- 18 (a) L. Zuppiroli, N. Papandreou and R. Kormann, *J. Appl. Phys.*, 1991, **70**, 246; (b) C. Wood and D. Emin, *Phys. Rev. B: Condens. Matter*, 1984, **29**, 4582.
- 19 L. J. Azevedo, E. L. Venturini, D. Emin and C. Wood, *Phys. Rev. B: Condens. Matter*, 1985, **32**, 7970.
- 20 O. Chauvet, D. Emin, L. Forro, T. L. Aselage and L. Zuppiroli, *Phys. Rev. B: Condens. Matter*, 1996, **53**, 14450.
- 21 T. L. Aselage, D. Emin, S. S. McCready and R. V. Duncan, *Phys. Rev. B: Condens. Matter*, 1998, **81**, 2316.
- 22 J. L. Hoard and R. E. Hughes, in *The Chemistry of Boron and Its Compounds*, ed. E. L. Muetterties, Wiley, New York, 1967, pp. 25.
- 23 (a) G. S. Zhdanov and N. G. Sevast'yanov, *C. R. Acad. Sci. URSS*, 1941, **32**, 432; (b) H. K. Clark and J. L. Hoard, *J. Am. Chem. Soc.*, 1943, **65**, 2115.
- 24 A. C. Larsen and D. T. Cromer, *Acta Crystallogr., Sect. A: Cryst. Phys., Diff., Theor. Gen. Cryst.*, 1972, **28**, S53.
- 25 (a) K. L. Walters and G. L. Green, *Quarterly Status Report on the Advanced Plutonium Fuels Program*, Los Alamos Scientific Laboratory, Los Alamos, 1970, pp. 14; (b) A. Kirfel, A. Gupta and G. Will, *Acta Crystallogr., Sect. B: Struct. Crystallogr. Cryst. Chem.*, 1979, **35**, 1052.
- 26 T. M. Duncan, *J. Am. Chem. Soc.*, 1984, **106**, 2270.
- 27 F. Mauri, N. Vast and C. J. Pickard, *Phys. Rev. Lett.*, 2001, **87**, 085506.
- 28 (a) K. Shirai and S. Emura, *J. Phys.: Condens. Matter*, 1996, **8**, 10919; (b) K. Shirai and S. Emura, *J. Solid State Chem.*, 1997, **133**, 93.
- 29 (a) R. Lazzari, N. Vast, J. M. Besson, S. Baroni and A. Dal Corso, *Phys. Rev. Lett.*, 1999, **83**, 3230; (b) N. Vast, J. M. Besson, S. Baroni and A. Dal Corso, *Comput. Mater. Sci.*, 2000, **17**, 127.
- 30 A. C. Larsen, in *Boron Rich Solids*, ed. D. Emin, T. Aselage, C. L. Beckel, I. A. Howard and C. Wood, AIP, New York, 1986, pp. 109.
- 31 R. J. Nelmes, J. S. Loveday, R. M. Wilson, W. G. Marchall, J. M. Besson, S. Klotz, G. Hamel, T. L. Aselage and S. Hull, *Phys. Rev. Lett.*, 1995, **74**, 2268.
- 32 (a) H. J. Becher and F. Thevenot, *Z. Anorg. Allg. Chem.*, 1974, **410**, 274; (b) D. R. Tallant, T. L. Aselage, A. N. Campbell and D. Emin, *Phys. Rev. B: Condens. Matter*, 1989, **40**, 5649; (c) T. L. Aselage, D. R. Tallant and D. Emin, *Phys. Rev. B: Condens. Matter*, 1997, **56**, 3122.
- 33 C. Wood, D. Emin and P. E. Gray, *Phys. Rev. B: Condens. Matter*, 1985, **31**, 6811.
- 34 (a) T. L. Aselage, D. Emin and S. S. McCready, *Phys. Status Solidi B*, 2000, **218**, 255; (b) T. L. Aselage, D. Emin and S. S. McCready, *Phys. Rev. B: Condens. Matter*, 2001, **64**, 054302.
- 35 (a) D. Emin, in *Physics and Chemistry of Carbides, Nitrides and Borides*, ed. R. Freor, Kluwer Academic Publishers, The Netherlands, 1991, pp. 691; (b) J. Gieske, T. L. Aselage and D. Emin, in *Boron Rich Solids*, ed. D. Emin, T. L. Aselage, A. C. Switendick, B. Morosin and C. L. Beckel, AIP, New York, 1991, pp. 376.
- 36 G. A. Samara, D. Emin and C. Wood, *Phys. Rev. B: Condens. Matter*, 1985, **32**, 2315.
- 37 (a) C. W. Tucker, Jr and P. Senio, *Acta Crystallogr.*, 1955, **8**, 371; (b) H. L. Yakel, *Acta Crystallogr., Sect. B: Struct. Crystallogr. Cryst. Chem.*, 1975, **31**, 1797.
- 38 D. Emin, *Phys. Rev. B: Condens. Matter*, 1988, **38**, 6041.
- 39 (a) O. A. Golikova, *Phys. Status Solidi A*, 1979, **51**, 11; (b) O. A. Golikova, in *Novel Refract. Semicond. Symp. 1987*, ed. D. Emin, T. L. Aselage and C. Wood, Pittsburg, PA, 1987, vol. 97, pp. 177.
- 40 (a) R. Franz and H. Werheit, *Europhys. Lett.*, 1989, **9**, 145; (b) R. Franz and W. Werheit, *AIP Conf. Proc.*, 1990, **231**, 29.
- 41 D. Emin, *Phys. Today*, 1982, **35**, 34.
- 42 M. J. Frisch, G. W. Trucks, H. B. Schlegel, P. M. W. Gill, B. G. Johnson, M. A. Robb, J. R. Cheeseman, T. Keith, G. A. Peterson, J. A. Montgomery, K. Raghavachari, M. A. Al-Laham, V. G. Zakrzewski, J. V. Ortiz, J. B. Foresman, J. Cioslowsky, B. B. Stefanov, A. Nanayakkara, M. Callacombe, C. Y. Peng, P. Y. Ayala, W. Chen, M. W. Wong, J. L. Andres, E. S. Replogle, R. Gomberts, R. L. Martin, D. J. Fox, J. S. Binkley, D. J. Defrees, J. Baker, J. P. Stewart, M. Head-Gordon, C. Gonzalez and

- J. A. Pople, *GAUSSIAN 98 (Version 5.2)*, Gaussian Inc., Pittsburgh, PA, USA, 1995.
- 43 (a) B3LYP is Becke's three-parameter hybrid method with a LYP correlation functional: A. D. Becke, *J. Chem. Phys.*, 1993, **98**, 5648; (b) C. Lee, W. Yang and R. G. Parr, *Phys. Rev. B: Condens. Matter*, 1988, **37**, 785; (c) S. H. Vosko, L. Wilk and M. Nusair, *Can. J. Phys.*, 1980, **58**, 1200; (d) P. J. Stephens, F. J. Devlin, C. F. Chabalowski and M. J. Frisch, *J. Phys. Chem.*, 1994, **98**, 11623.
- 44 (a) G. Kresse and J. Hafner, *Phys. Rev. B: Condens. Matter*, 1993, **47**, 558; (b) G. Kresse and J. Hafner, *Phys. Rev. B: Condens. Matter*, 1994, **49**, 14251; (c) G. Kresse and J. Hafner, *Phys. Rev. B: Condens. Matter*, 1996, **54**, 11169.
- 45 R. Hoffmann, *J. Chem. Phys.*, 1963, **39**, 1397.
- 46 G. A. Landrum and W. V. Glassy, *YAcHMOP (Version 3.01)*. (Freely available at <http://yaehmop.sourceforge.net>).
- 47 R. Hughbanks and R. Hoffmann, *J. Am. Chem. Soc.*, 1983, **105**, 3528.
- 48 G. Kresse and J. Hafner, *Phys. Rev. B: Condens. Matter*, 1999, **59**, 1758.
- 49 J. P. Perdew and Z. Zunger, *Phys. Rev. B: Condens. Matter*, 1981, **23**, 5048.
- 50 H. J. Monkhorst and J. Pack, *Phys. Rev. B: Solid State*, 1976, **13**, 5188.
- 51 In reality there will be *exo*-polyhedral and polyhedral orbital mixing to the extent symmetry allows it.
- 52 (a) K. Wade, *Chem. Commun.*, 1971, 792; (b) K. Wade, *Adv. Inorg. Chem. Radiochem.*, 1976, **18**, 1.
- 53 M. M. Balakrishnarajan, R. Hoffmann, P. D. Pancharatna and E. D. Jemmis, *Inorg. Chem.*, 2003, **42**, 4650.
- 54 T. Peymann, C. B. Knobler, S. I. Khan and M. F. Hawthorne, *Angew. Chem., Int. Ed.*, 2001, **40**, 1664.
- 55 (a) M. L. McKee, *Inorg. Chem.*, 2002, **41**, 1299; (b) M. L. McKee, *Inorg. Chem.*, 1999, **38**, 321; (c) L. A. Boyd, W. Clegg, R. C. B. Copley, M. G. Davidson, M. A. Fox, T. G. Hibbert, J. A. K. Howard, A. Mackinnon, R. J. Peace and K. Wade, *Dalton Trans.*, 2004, 2786.
- 56 (a) M. M. Balakrishnarajan and R. Hoffmann, *Angew. Chem., Int. Ed.*, 2003, **42**, 3777; (b) M. M. Balakrishnarajan and R. Hoffmann, *Inorg. Chem.*, 2004, **43**, 27.
- 57 M. Baudler, K. Rockstein and W. Oehlert, *Chem. Ber.*, 1991, **124**, 1149.
- 58 D. R. Huntley, G. Markopoulos, P. M. Donovan, L. T. Scott and R. Hoffmann, *Angew. Chem., Int. Ed.*, 2005, **45**, 7549.